Water Science & Technology

IWA PUBLISHING

Water Science & Technology Vol 87 No 3, 798 doi: 10.2166/wst.2023.007

Preparation of CaMgAl-calcined layered double hydroxides and application on the removal of phosphates

Liping Xiao[a,*], Zhemeng Wang[b], Dongxue Wang[a], Yunlong Lan[a] and Qiaoping Kong[a]

[a] School of Environmental and Municipal Engineering, Qingdao University of Technology, Qingdao 266520, PR China
[b] School of Civil Engineering, Liaoning Technical University, Fuxin 123000, PR China
*Corresponding author. E-mail: xiaoliping@qut.edu.cn

ABSTRACT

A calcined CaMgAl-layered double hydroxide nanocomposite, CaMgAl-LDH (CCMA-0.83-600), was prepared by introducing Mg on the basis of CaAl-LDHs for the removal of phosphate from wastewater. The structure of the as-synthesized CCMA-0.83-600 was confirmed by XRD and SEM analyses. Parameters affecting the adsorption process of phosphate adsorbed by CCMA-0.83-600 were thoroughly explored, such as initial pH, adsorbent dosage and co-existing anions. The adsorption kinetic study suggested that the adsorption process accorded with the pseudo-second-order kinetic model and the adsorption rate was controlled by both the liquid film diffusion and intra-particle diffusion. The adsorption isotherm study indicated the adsorption process followed by the Langmuir isotherm model. Thermodynamic analysis suggested that the adsorption of phosphate was spontaneous and exothermic. The obtained results indicated that CCMA-0.83-600 is a suitable candidate for the removal of phosphate from wastewater.

Key words: adsorption, LDHs, mechanism, phosphates, wastewater

HIGHLIGHTS

- Ternary metal-LDHs (CCMA-0.83-600) were synthesized for adsorbing phosphate.
- The adsorption of phosphate by CCMA-0.83-600 is a chemical and monolayer process.
- Phosphate was bound by CCMA-0.83-600 via the synergistic effect of multiple forces.

GRAPHICAL ABSTRACT

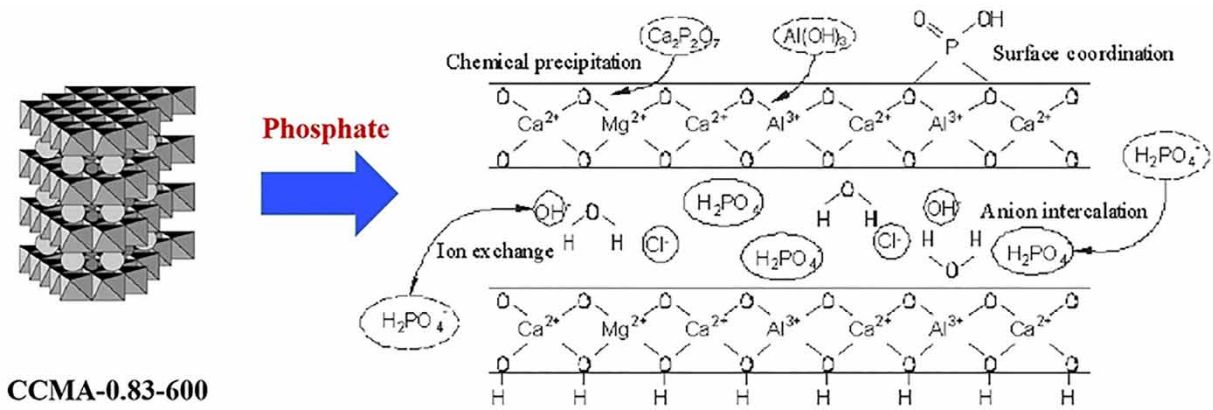

1. INTRODUCTION

Phosphorus is an essential element for the growth of algae and other organisms (Wang *et al.* 2020). High level of phosphorus discharged from wastewater into natural water not only results in algae blooms but also triggers eutrophication (Cao *et al.* 2020), posing a potential threat to the ecosystem. Thus, it is crucial to develop efficient methods and materials for phosphorus

removal. Various treatment technologies, such as membrane separation, ion exchange, electrodialysis, chemical precipitation, adsorption and biological methods, have been employed to recover phosphorous from wastewater. Among them, the adsorption method, with the advantages of easy operation, low cost and stabilizing effect, is considered a promising separation technique for the removal of phosphorus. The core of the adsorption method is to find an adsorbent with excellent adsorption performance (Kong *et al.* 2021, 2022). To date, a large number of adsorbents, such as metal oxide hydroxides, diatomite, kaolin, lignite, bentonite and layered double hydroxides (LDHs), have been successfully adopted for adsorbing phosphorous (Seftel *et al.* 2018; Guo *et al.* 2021; Khajeh *et al.* 2022).

LDH with large surface areas and easily exchangeable interlayer ions is called anionic clay. The general chemical formula of LDH is $[M^{2+}_{1-x}M_x{}^{3+}(OH)_2]X^+(A^{n-})_{x/n}{\cdot}mH_2O$, where M^{2+} and M^{3+} are divalent and trivalent metal cations, respectively, A^{n-} is the interlaminar anion, x is the molar ratio of $M^{3+}/(M^{3+}+M^{2+})$ and m is the number of interlaminar water molecules (Li *et al.* 2016). Nowadays, LDHs are employed in adsorbing various pollutants such as phosphorus, nitrate, acid yellow, perfluorooctanoic acid, tetracycline hydrochloride, Pb^{2+}, Cr(VI), SeO_4^{2-} and so on. Phosphorus mainly exists in the form of organic phosphate, orthophosphate and polyphosphate in wastewater (Cao *et al.* 2020) and the phosphorus concentration in different wastewater will be different. Organic phosphate and polyphosphate can be decomposed into orthophosphate due to bacteria. So the key to phosphorus removal is how to remove orthophosphate from wastewater. As adsorbents, LDHs have exhibited excellent adsorption ability towards phosphate. For example, our team's previous work showed that CR-LDH (AlCa-LDHs) prepared from the industrial waste of calcium carbide slag and red mud exhibited 16.6 mg/g phosphate adsorption capacity by CR-LDH (Xiao *et al.* 2021). Ca released from CR-LDH would enhance the adsorption of phosphate by co-precipitation. CR-LDH was deemed as a potential adsorbent for the treatment of phosphate-containing wastewater and the COD, turbidity and NH_4^+-N of practical wastewater treated by CR-LDH could be reduced by 42.39, 77.20 and 20.71%, respectively. Li *et al.* (2016) investigated the ratio of Mg/Al on the adsorption behavior of Mg/Al-LDHs biochar for phosphate. Experimental results indicated that the increase of the Mg/Al ratio in adsorbent will improve phosphate adsorption and the maximum adsorption capacity of Mg/Al-LDHs biochar toward phosphate calculated by the Langmuir isotherm model was 81.83 mg/g within the Mg/Al ratio of 4:1 in Mg/Al-LDHs biochar (pH 3.0). Ion exchange, electrostatic attraction and surface inner-sphere complex formation were the main adsorption mechanism for phosphate adsorbed by Mg/Al-LDHs biochar. Literature research found that binary metal-LDHs, such as MgAl-LDHs and CaAl-LDHs, achieved good adsorption performance toward phosphate. To our best knowledge, although ternary metal-LDH is reported in adsorbing HCl (Wu *et al.* 2019), As(III), Cd(II) (Lyu *et al.* 2022) and triphosphate (Zhou *et al.* 2011), in removing phosphate in wastewater are little explored, especially for CaMgAl-LDHs. The adsorption performance and mechanism of CaMgAl-LDHs with respect to phosphate were unclear that needed to be explored further.

In the current work, ternary metal-LDHs (CaMgAl-LDHs) were synthesized by introducing the Mg element to the basis of CaAl-LDHs. The obtained CaMgAl-LDHs were further calcined to prepare CaMgAl-calcined LDHs under different calcination temperatures. The CaMgAl-calcined LDH composite was investigated using XRD, SEM and FT-IR. Batch adsorption experiments, under different initial solution pH values, adsorbent dosage and competitive anions, were conducted to determine the adsorption characters and adsorption abilities and phosphate onto the CaMgAl-calcined LDHs. The adsorption kinetic, isotherm and thermodynamic analysis were conducted to reveal the interaction between CaMgAl-calcined LDHs and phosphate.

2. MATERIALS AND METHODS

2.1. Chemicals and materials

NaCl, $MgCl_2{\cdot}6H_2O$, $CaCl_2$, $Al(NO_3)_3{\cdot}9H_2O$ and ascorbic acid were provided by Sinopharm, China. KH_2PO_4 was obtained from Liaoning Quanrui Reagent Co., Ltd, China. Phosphorus standard solution (GSB04-1741-2004a) with a concentration of 100 mg/L was purchased from the national center for analysis and testing of nonferrous metals and electronic materials, China. All reagents used were of analytic grade, except as noted.

2.2. Preparation of CaMgAl-LDHs and CaMgAl-calcined LDHs

The CaMgAl-LDHs were synthesized by a co-precipitation method. The detailed preparation procedure is as follows. First, certain amounts of $CaCl_2$, $MgCl_2{\cdot}6H_2O$, $Al(NO_3)_3{\cdot}9H_2O$ were dissolved by deionized water to obtain a mixed metal salt solution with the molar ratio of divalent metal cations (Ca^{2+} and Mg^{2+}) to trivalent metal cations (Al^{3+}) of 3 and $X=[n(Ca^{2+})/n(Ca^{2+}+Mg^{2+})]=0.83$. Then, 250 mL of the above-mixed metal salt solution and 1 mol/L NaOH solution were added

dropwise to 200 mL of the 0.5 mol/L NaCl solution, maintaining the pH of the solution around 9–13. After the titration was completed, the above-mixed solution was stirred at 35–75 °C for another 30 min. Subsequently, the precipitate was crystallized in a water bath at 70 °C for 24 h. The crystallized precipitate was separated by centrifugation, washed with deionized water and dried at 110 °C for 24 h to obtain CaMgAl-LDHs. After that, the ground CaMgAl-LDH samples were calcined at 300–800 °C for 4 h to obtain CaMgAl-calcined LDHs. Finally, the CaMgAl-calcined LDHs were ground to pass through the 200-mesh sieve and then placed in the dryer for further experiments. The corresponding calcined CaMgAl-LDHs are named CCMA-0.83-Y (Y represented the roasting temperature).

2.3. Characterization

Powder X-ray diffraction (XRD) patterns were recorded on a Bruker D8 Advance X-ray diffractometer with Cu Kα radiation ($\lambda = 1.5418$ Å) at 40 KV, 40 mA, a 2θ angle in the range of 5°–70° and a step size of 0.02°/s. The surface morphology was measured with a QUANTA 250 scanning electron microscope (SEM). The adsorbent was pelletized with KBr for the FT-IR analysis using a TENSOR27 infrared spectrometer with 4 cm^{-1} resolution in the range of 4,000–400 cm^{-1}.

2.4. Adsorption experiments

The batch adsorption test was conducted in a 250 mL Erlenmeyer flask installed in a shaker with a shaking speed of 200 rpm at 25 °C. A certain amount of adsorbent was immersed into 100 mL of the phosphate solution with a concentration ranging from 10 to 300 mg/L. After adsorption for equilibrium, the supernatant was taken from the reaction system and then filtered through a 0.45 μm membrane filter for further analysis by the molybdate colorimetric method (Xiao *et al.* 2021). The initial pH values of the solutions were adjusted by 0.1 mol·L^{-1} NaOH and HNO_3. The adsorption amount and removal efficiency of phosphate onto adsorbent were calculated as Equations (1) and (2).

$$q = \frac{(C_0 - C_t)V}{m} \tag{1}$$

$$\text{Removal efficiency} = \frac{C_0 - C_t}{C_0} \times 100\% \tag{2}$$

where q represents the adsorption amount of phosphate onto adsorbent, mg/g; C_0 is the initial concentration of phosphate, mg/L; C_t denotes the concentration of phosphate at time of t, mg/L; V is the volume of phosphate solution, L, and m is the adsorbent dosage, g.

Especially, in an adsorption kinetic test, 0.16 g CCMA-0.83-600 was immersed into 200 mL of phosphate solution with a concentration of 200 mg/L in a 500 mL conical flask. The conical flask was shaken at the rate of 200 rpm at 25 °C. At each sampling time (e.g., 5, 10, 30, 60, 120, 180, 240, 300, 360, 420, 480 min), 5 mL of the uniformly mixed solution was taken from the conical flask and then filtrated for further analysis.

The adsorption kinetic of phosphate adsorbed by CCMA-0.83-600 was addressed by adding 0.08 g CCMA-0.83-600 into 100 mL of the phosphate solution with a concentration ranging from 20 to 500 mg/L in the 100 mL conical flask. The conical flasks were then shaken for 24 h at 25 °C. As for the thermodynamic test, the adsorbate-adsorbent system reacted at 15, 25 and 35 °C.

3. RESULTS AND DISCUSSION

3.1. The preparation of CCMA-0.83-600

3.1.1. The effect of co-precipitation temperature

The effect of co-precipitation temperature on the XRD patterns of CCMA-0.83 and the adsorption performance of phosphate were investigated with co-precipitation temperature in the range of 35–75 °C and the results are exhibited in Figure 1. As shown in Figure 1(a), the characteristic peaks of (002), (004), (112), (020) and (−316) crystal planes of boehmite appeared in the XRD pattern of CCMA within co-precipitation temperatures at 45, 55, 65 and 75 °C. Almost no impurity peak was found in the XRD patterns of 45, 55 and 65 °C, and the diffraction peak of the (002) crystal face corresponding to the low 2θ zone was relatively sharp with high symmetry, indicating that the prepared samples had been crystallized into a complete monoclinic symmetric layered structure. According to Figure 1(b), the adsorption performance of CCMA-0.83-400 increased with a higher co-precipitation temperature, it reached 90.67 mg/g maximum at a co-precipitation temperature of 65 °C and

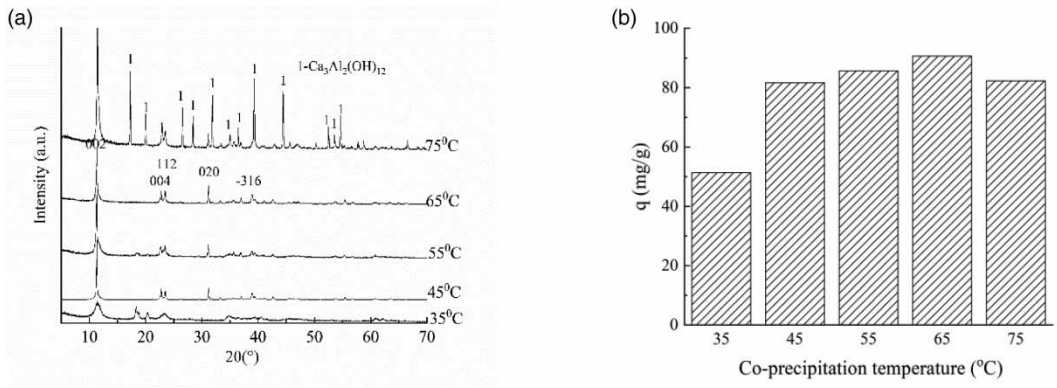

Figure 1 | (a) Effect of co-precipitation temperature on the XRD patterns and (b) adsorption capacity of CCMA-0.83-600 toward phosphate.

with a further increase in co-precipitation temperature, phosphate adsorption decreased because CMA-0.83 contained $Ca_3Al_2(OH)_{12}$ heterophase within a co-precipitation temperature of 75 °C.

3.1.2. The effect of co-precipitation pH

The effect of co-precipitation pH on the XRD patterns of CCMA-0.83 and the adsorption performance of phosphate were investigated with co-precipitation pH varied from 9 to 13 and the results are exhibited in Figure 2. As shown in Figure 2(a), when the co-precipitation pH was 10, only the characteristic peak of boehmite appeared in the product was the pure boehmite mineral phase. At a pH of 10, the obtained product contained a sharp peak type, good symmetry, low and flat baseline and good crystallization performance. According to Figure 2(b), the adsorption capacity of CCMA-0.83-600 with respect to phosphate was first increased and then decreased with the increase of co-precipitation pH. A maximum phosphate adsorption amount of 90.67 mg/g was achieved at a pH of 10 and the corresponding adsorbent was pure boehmite mineral phase without impurities. Combined with the XRD results, it could be inferred that the calcined products would be different within different co-precipitation pH, which would lead to different adsorption performances. Thus, the optimum co-precipitation pH of CCMA-0.83-400 was 10.

3.1.3. The effect of calcination temperature

The effect of calcination temperature on the XRD patterns of CCMA-0.83 is shown in Figure 3(a). When the calcination temperature was in the range of 300–500 °C, the XRD diffraction peak of CCMA-0.83 was relatively broad and inconspicuous, indicating that the hydroxyl groups in the interlayer of CMA-0.83 were being removed, and the lamellar structure of the crystal began to collapse and transform into an amorphous form. When the calcination temperature was raised to 600 °C, the

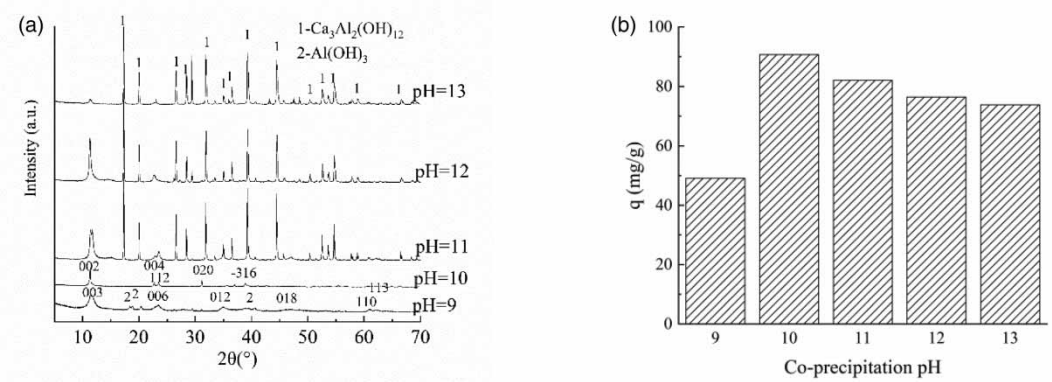

Figure 2 | (a) Effect of co-precipitation pH on the XRD patterns and (b) adsorption capacity of CCMA-0.83-600 toward phosphate.

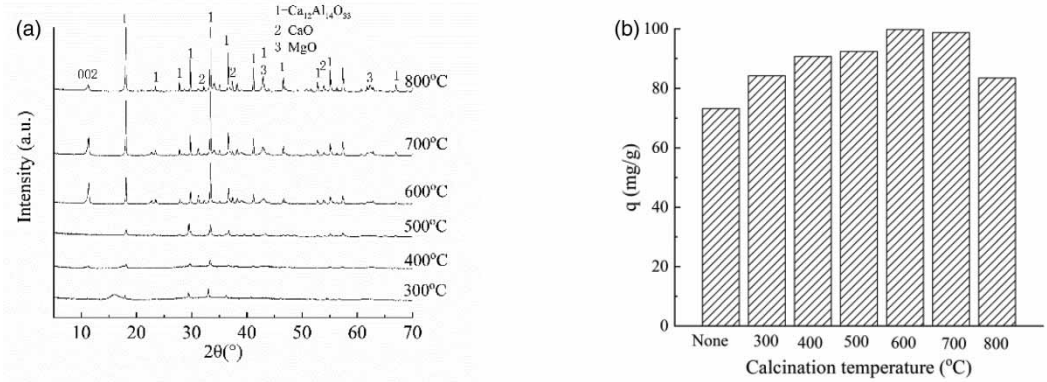

Figure 3 | (a) Effect of calcination temperature on the XRD patterns and (b) adsorption capacity of CCMA-0.83-600 toward phosphate.

calcination products were gradually transformed into $Ca_{12}Al_{14}O_{33}$, MgO and CaO mineral phases. Curves d, e and f in Figure 4(a) exhibit characteristic peaks corresponding to the crystal plane of (002) at about $2\theta = 11.3$, which was mainly due to the structural memory effect that made CCMA-0.83 absorb moisture in the air and partially restore the layered state structure.

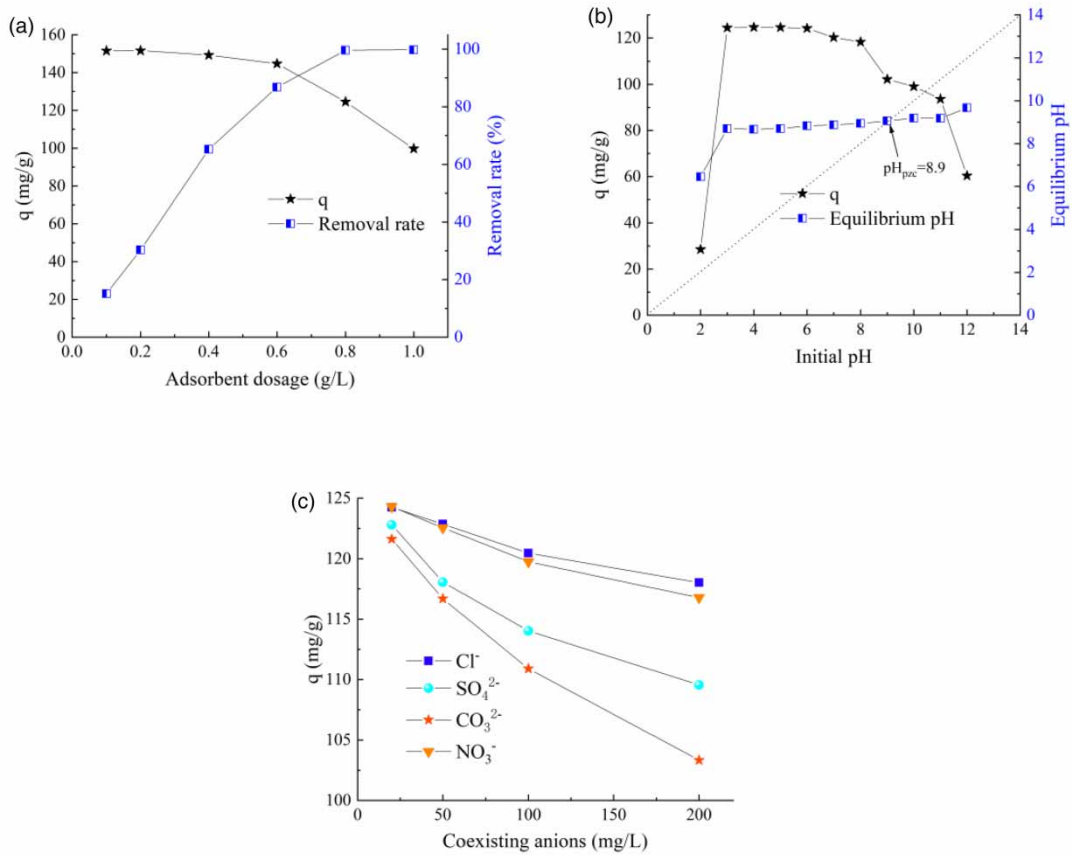

Figure 4 | Adsorption performance of CCMA-0.83-600 with respect to phosphate as a function of adsorbent dosage (a), initial pH (b) and co-existing anions (c).

The effect of calcination temperature on the adsorption of phosphate is given in Figure 3(b). It can be seen that the adsorption ability of CCMA-0.83 toward phosphate was better than that of CMA-0.83. As the calcination temperature was increased from 300 to 800 °C, the adsorption ability of CCMA-0.83 with respect to PO_4^{3-} was first increased and then decreased. A maximum adsorption amount of 99.75 mg/g was achieved at a calcination temperature of 600 °C. This phenomenon was might be attributed to the structural memory effect. When the calcination temperature was in the range of 300–600 °C, part to all of the layered structure of CCMA-0.83 was collapsed and the hydroxyl groups were removed. Thus, the adsorption ability of CCMA-0.83 toward phosphate was enhanced due to the reduction of ions competing within PO_4^{3-} in the interlayer. When the calcination temperature was higher than 600 °C, the adsorption capacity of phosphate was decreased because the high calcination temperature destroyed the structure memory effect which could be confirmed by XRD results (Figure 3(a)). The most favorable calcination temperature was 600 °C.

Based on the above results, the optimum conditions for the preparation of CCMA-0.83-600 were as follows: co-precipitation temperature of 65 °C, co-precipitation pH of 10 and calcination temperature of 600 °C.

3.2. Factors affecting CCMA-0.83-600 adsorption of phosphate

3.2.1. Effect of adsorbent dosage

The effect of adsorbent dosage on the adsorption behavior of CCMA -0.83-600 is investigated with an adsorbent dosage ranging from 0.1 to 1.0 g/L and the result is shown in Figure 4(a).

In general, a high CCMA-0.83-600 dosage achieved a high phosphate removal because a more active adsorption site would be available to bind phosphate in the aqueous solution. Most notably, CCMA-0.83-600 presented a two-phase adsorption curve in phosphate adsorption as the increase of CCMA-0.83-600 dosage. With the dosage of CCMA-0.83-600 increased from 0.1 to 0.8 g/L, the removal rate sharply increased from 15.15 to 99.62%. However, when the CCMA-0.83-600 dosage was higher than 0.8 g/L, the phosphate removal rate hardly increased and the tangent slope of the curve decreased to almost 0. Conversely, the adsorption capacity of CCMA-0.83-600 exhibited a different trend with the increase of CCMA-0.83-600 dosage. With the increase in CCMA-0.83-600 dose, more phosphate was removed from the solution, and the residual phosphate got lower. Correspondingly, the concentration gradient was getting smaller, leading to the difficulty in phosphate adsorption. It peaked at 124.53 mg/g at 0.8 g/L of CCMA-0.83-600. In the subsequent tests, the dosage of CCMA-0.83-600 used was 0.8 g/L.

3.2.2. Effect of the initial solution pH

The effect of the initial solution pH (2.0–12.0) on CCMA-0.83-600 adsorption of phosphate is presented in Figure 4(b). At pH of 2, the adsorption ability of CCMA-0.83-600 was relatively low. When the pH value was at a relatively low level, H_3PO_4 and $H_2PO_4^-$ were the main species of P. At this time, CCMA-0.83-600 would be dissolved and couldn't be restored to the layered structure. The removal of phosphate was mainly through the precipitation reaction formed between the dissolved Ca^{2+}, Mg^{2+}, Al^{3+} and phosphate. The adsorption amount was increased from 28.51 to 124.39 mg/g when the initial solution pH increased from 2 to 3. CCMA-0.83-600 remained a relatively high phosphate adsorption ability in the range of pH 3–8, and a maximum phosphate adsorption amount of 124.59 mg/g was achieved at a pH of 4. Meanwhile, the point of zero charge (pH_{pzc}) of CCMA-0.83-600 was 8.9. When the solution pH $<$ pH_{pzc}, the surface of CCMC-0.83-600 became protonated and more positively charged with the decrease in pH, favoring the adsorption of phosphate. At pH above pH_{pzc}, the deprotonation reaction led to the intensification of competition between phosphate ions and OH^-, resulting in the lower removal of phosphate. At a higher pH, the main species of phosphate in the aqueous solutions were PO_4^{3-}, HPO_4^{2-} and $H_2PO_4^-$ (Cheng *et al.* 2009; Zhang *et al.* 2019). More hydroxyl groups would be on the layer, enhancing the coordination between metal ions and phosphate. Besides, the positive charge of the laminate would be reduced, weakening the electrostatic adsorption ability. The solution pH remained between 8.6 and 9.2 after the equilibrium of the adsorption reaction, indicating that CCMA-0.83-600 had a certain regulating effect on the pH of the solution, that is, CCMA-0.83-600 in OH^- was released during the recombination, and part of the OH^- would be adsorbed by CCMA-0.83-600 after the recombination was completed. Based on the above results, a pH of 4 will be selected in a further study.

3.2.3. Effect of co-existing anions

The effect of co-existing anions on the adsorption of phosphate is investigated with Cl^-, NO_3^-, CO_3^{2-} and SO_4^{2-} as background anions and the results are shown in Figure 4(c). The concentration of the above four co-existing anions was 20, 50, 100 and

200 mg/L. Cl^-, NO_3^-, CO_3^{2-} and SO_4^{2-} could significantly influence the adsorption of CCMA-0.83-600 with respect to phosphate, showing strong competitive adsorption with phosphate at pH 4.0. The suppression of phosphate adsorption was enhanced by increasing the concentration of Cl^-, NO_3^-, CO_3^{2-} and SO_4^{2-} ions from 20 to 200 mg/L. The inhibition order of the above four background anions was following the sequence of $CO_3^{2-} > SO_4^{2-} > NO_3^- > Cl^-$. The co-existing anions will enter the interlayer of CaMgAl-LDHs and occupy part of interlayer adsorption sites, reducing the adsorption ability of CCMA-0.83-600 toward phosphate. A strong force existed between the anion with high valence and the positively charged layer, making it easier to enter the interlayer channel. Thus, the inhibitory effect of CO_3^{2-} and SO_4^{2-} dianions was stronger than that of NO_3^- and Cl^- monovalent anions (Xiao *et al.* 2021).

3.2.4. Kinetic study

To determine the suitable contact time needed to reach equilibrium and illustrate the adsorption rate, the phosphate adsorption performance of CCMA-0.83-600 was investigated as a function of reaction time at 25 °C, and the result is shown in Figure 5. For CCMA-0.83-600 at a phosphate concentration of 100 mg/L, equilibrium was reached after 360 min. As shown in Figure 5, rapid adsorption was obtained during the initial stage of 0–60 min, which was because of the abundance of active adsorption sites and phosphate in the aqueous solution. Subsequently, a slow adsorption stage of 60–360 min was followed. Finally, it is an equilibrium stage after 360 min, at which time there were relatively few phosphate ions in the solution. Thus, 360 min was suitable for the adsorption of phosphate.

Subsequently, to interpret the adsorption kinetics of CCMA-0.83-600 toward phosphate, several models including pseudo-first-order (Equation (3)) and pseudo-second-order kinetic (Equation (4)) models are used to fit the experimental data and the results are shown in Figure 5(a) and Table 1. Clearly, R^2 of the pseudo-second-order expression ($R^2 = 0.993$) exceeded that of

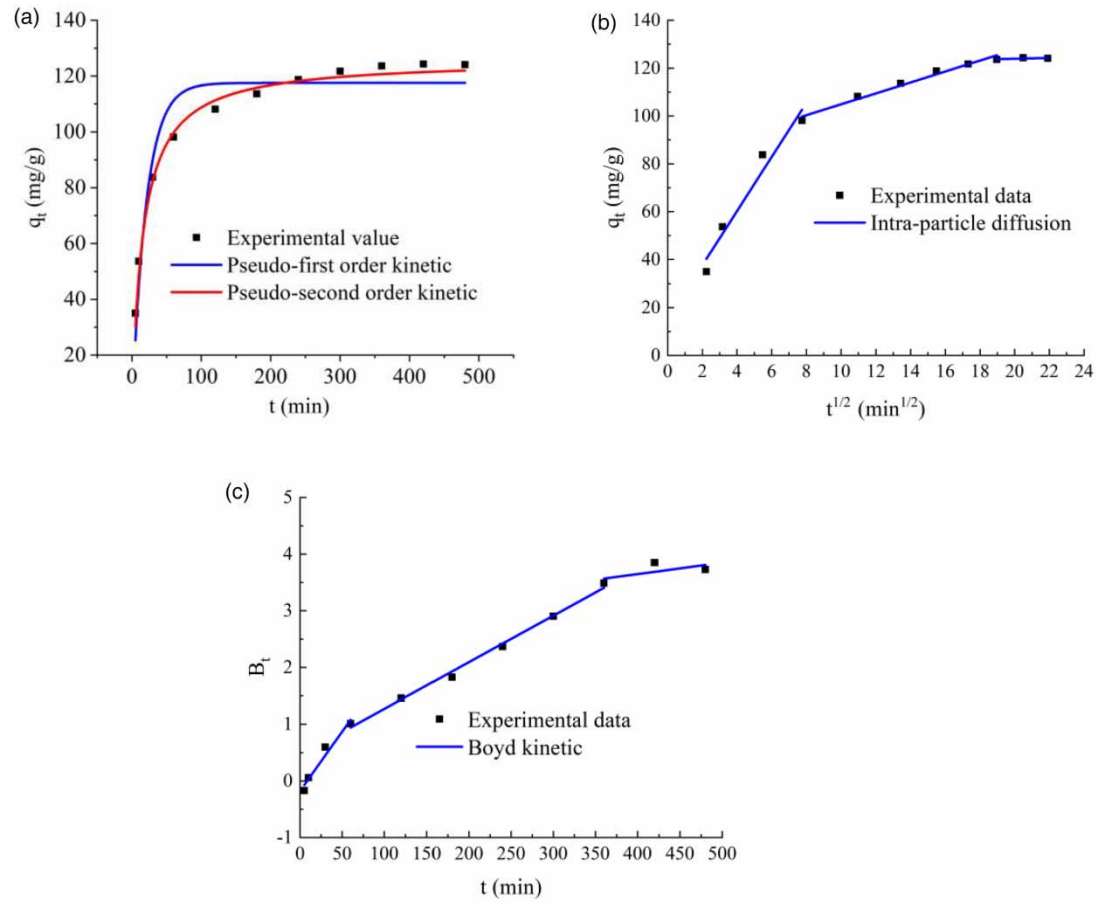

Figure 5 | Fitting results of the pseudo-first-order model, and the pseudo-second-order kinetic model (a), the intra-particle diffusion model (b) and the Boyd kinetic model (c).

Table 1 | Fitting results of kinetic model

Kinetic model	Parameter	Value
Pseudo-first-order kinetic model	Q_e	117.55
	k_1	0.0485
	R^2	0.946
Pseudo-second-order kinetic model	Q_e	125.94
	k_2	0.0005
	R^2	0.993
Intra-particle diffusion model	C_1	14.955
	R_1^2	0.958
	k_{31}	11.317
	C_2	82.092
	k_{32}	2.218
	R_2^2	0.979
	C_3	118.99
	k_{33}	0.245
	R_3^2	0.958

the pseudo-first-order expression ($R^2 = 0.946$), suggesting that the pseudo-second-order kinetic model was more suitable to describe the experimental data of phosphate adsorbed by CCMA-0.83-600 ($R^2 = 0.993$). The experimental adsorption capacity value was also consistent with the Q_e value (125.94 mg/g) calculated from the pseudo-second-order kinetic model. It could further interpret that the removal of phosphate was dominated by chemical adsorption through chemical binding between the active adsorption sites of CCMA-0.83-600 and phosphate.

$$q_t = q_e(1 - e^{-k_1 t}) \tag{3}$$

$$q_t = \frac{q_e^2 k_2 t}{1 + q_e k_2 t} \tag{4}$$

where q_e (mg/g) and q_t (mg/g) are the amounts of phosphate adsorbed at equilibrium and at time t, k_1 (min^{-1}) and k_2 (g/mg/min) are the rate constants of pseudo-first-order and pseudo-second-order models of adsorption, respectively.

To further explore the involvement of intra-particle behavior in the adsorption process of phosphate adsorbed by CCMA-0.83-600, the intra-particle diffusion model was adopted to fit the experimental data and the results are shown in Figure 5(b) and Table 1. The equation of the intra-particle diffusion model is as follows:

$$q_t = k_3 t^{1/2} + C \tag{5}$$

where k_3 is the intra-particle diffusion rate constant ($\text{mg/g/min}^{1/2}$) and C is the constant related to the thickness of the boundary layer, and its value is the y-axis intercept (mg/g).

According to the intra-particle diffusion model, the diffusion phenomenon participated in the adsorption process when Q_t vs $t^{1/2}$ was a linear plot. Furthermore, if the intercept of the obtained plot was zero, this suggests that the only rate-controlling step in the adsorption process was intra-particle diffusion. Given that the experimental data fitted by the intra-particle diffusion model (Q_t vs $t_{1/2}$) plot showed multi-linearity, the adsorption process of phosphate adsorbed by CCMA-0.83-600 was controlled by more than one mechanism. Three-stage adsorption processes are presented in Figure 5(b). Stage I (0–60 min) is a fast adsorption phase. If a large number of free adsorption sites were available on the surface of CCMA-0.83-600, the phosphate would reach the surface of the adsorbent through liquid membrane diffusion and then could be quickly adsorbed. Stage II (60–360 min), intra-particle diffusion phase, was a rate-limiting step. Most of the active sites on the surface of CCMA-0.83-600 were occupied by phosphate, the phosphate anions diffused onto the surface of CCMA-0.83-600 through the liquid film would enter the inside adsorption sites through intra-particle diffusion. Stage III (>360 min) is the adsorption equilibrium stage. The constant C comprised $C_{31} < C_{32} < C_{33}$, suggesting an increase in the thickness of the boundary layer with the proceeding of adsorbing adsorbate.

To further explore the actual slow step in the adsorption process (Manobala *et al.* 2021), the Boyd kinetic model is adopted to fit the experimental data and the results are given in Figure 5(c).

$$F = 1 - \frac{6}{\pi^2}\exp^{-B_t} \tag{6}$$

$$B_t = -0.4977 - \ln\left(1 - \frac{q_t}{q_e}\right) \tag{7}$$

where F is the solute fraction of adsorbate at time t and B_t is the mathematical function of F.

As shown in Figure 5(c), the Boyd kinetic plots were linear and did not pass through the origin, indicating that the film diffusion or external mass transport mechanism occupied predominated status and the rate-determining step in the adsorption reaction is the external mass transfer (Manobala *et al.* 2021).

3.2.5. Adsorption isotherm studies

The influence of initial adsorbate concentration on the adsorption behavior of CCMA-0.83-600 toward phosphate is further investigated at different temperatures and the results are shown in Figure 6. The adsorption capacity of CCMA-0.83-600 with respect to phosphate increases with the increasing initial phosphate concentration and eventually plateaus. At 25 °C, the adsorption capacities of CCMA-0.83-600 reached almost 149.26 mg/g and the phosphate removal rate was 99.62%, as the dosage of CCMA-0.83-600 was 0.8 g/L and the initial phosphate concentration was 100 mg/L. At this time, the phosphate concentration in the effluent was 0.38 mg/L which met the first-class discharge standard (≤0.5 mg/L) in the comprehensive wastewater discharge standard of China (GB8978-1996).

Langmuir and Freundlich adsorption isotherms are adopted to investigate the equilibrium relationship between phosphate anchored on CCMA-0.83-600 and the phosphate remaining in the solution. The present experimental data were fitted by the Langmuir adsorption isotherm model Equation (4) and the Freundlich adsorption isotherm model Equation (5) as follows.

The Langmuir equation model:

$$q_e = \frac{q_{\max} K_L C_e}{1 + K_L C_e} \tag{8}$$

The Freundlich equation model:

$$q_e = K_F C_e^{\frac{1}{n}} \tag{9}$$

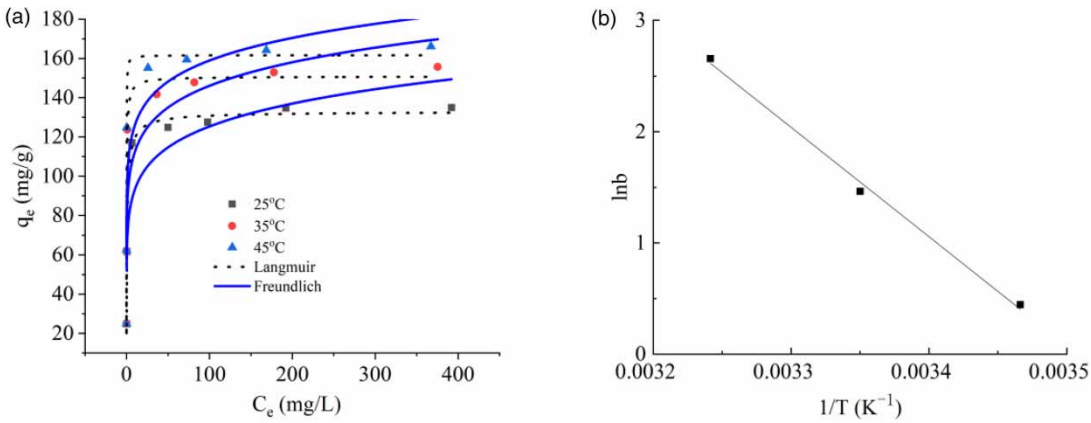

Figure 6 | Isotherms of phosphate adsorption on CCMA-0.83-600 (a) and lnb and 1/*T* relationship curve of phosphate adsorbed by CCMA-0.83-600 (b).

where q_{max} (mg/g) represents the theoretical maximum adsorption capacity, K_L (L/g) and K_F (L/g) are the Langmuir and Freundlich adsorption affinity constants, respectively, and $1/n$ is the adsorption intensity of the Freundlich model. The Langmuir and Freundlich isotherm plots for phosphate onto CCMA-0.83-600 are given in Figure 6.

As displayed in Figure 6 and Table 2, the regression coefficient values determined by the Langmuir isotherm model were the highest, suggesting that the adsorption of phosphate by CCMA-0.83-600 was best fitted with the Langmuir isotherm model ($0.991 \leq R^2 \leq 0.994$). Thus, phosphate adsorbed by CCMA-0.83-600 was a homogeneous monolayer adsorption process. The theoretical maximum adsorption capacity of CCMA-0.83-600 obtained by the Langmuir isotherm model was basically consistent with the experimental data. As the reaction temperature increased from 15 to 35 °C, the theoretical maximum adsorption capacity determined by the Langmuir model was increased from 130.79 to 161.66 mg/g, indicating that the increased temperature was conducive to the adsorption of phosphate by CCMA-0.83-600. According to the Freundlich model, the n value was greater than 1, suggesting that the adsorption process of phosphate by CCMA-0.83-600 was favorable.

3.2.6. Adsorption thermodynamics

Adsorption thermodynamics analysis was also used to evaluate the adsorption process of phosphate adsorbed by CCMA-0.83-600 and the results are shown in Figure 6(b) and Table 3. The adsorption thermodynamic formula is expressed as follows (Zhang *et al.* 2021):

$$\Delta G = -RT\ln K \tag{10}$$

$$\ln K = \frac{\Delta S}{R} - \frac{\Delta H}{RT} \tag{11}$$

where ΔG represents the Gibbs free energy, kJ/mol; R represents the is the constant of perfect gas and $R = 8.314$ J/mol/K; T is the absolute temperature of the solution, K; ΔS is the entropy change, J/mol/K; ΔH is the enthalpy change, kJ/mol and K represent the standard equilibrium constants. Because the adsorption process of CC-MA-0.83-600 toward phosphate fitted the Langmuir isotherm model well with $R^2 > 0.99$, the Langmuir constant of b could be calculated as K.

The negative $\triangle G$ values indicated that the adsorption of phosphate by CCMA-0.83-600 was a spontaneous process. As the temperature increased from 15 to 35 °C, the $\triangle G$ decreased from −1.07 to −6.82 kJ/mol, suggesting that the adsorption of phosphate was an endothermic reaction. The positive $\triangle H$ suggested the adsorption of phosphate was endothermic. The $\triangle S$ value was positive, indicating the increase in randomness and affinity in phosphate adsorbed by CCMA-0.83-600.

3.2.7. Adsorption mechanisms

The adsorption of phosphate onto CCMA-0.83-600 was a complicated process which might involve various specific mechanisms including physical adsorption, anion intercalation, ion exchange, surface coordination and chemical precipitation. (1) Physical adsorption: CCMA-0.83-600, one kind of LDHs, has good lamellar structure. It can be seen from Figure 7 that

Table 2 | Isotherm fitting results of phosphorus removal by CCMA-0.83-600

	Langmuir			Freundlich		
Temperature (K)	Q_{max} (mg/g)	K_L	R^2	K_F	n	R^2
288.15	130.79	1.56	0.992	69.35	7.78	0.832
298.15	149.91	4.32	0.991	86.45	8.78	0.822
308.15	161.66	14.26	0.994	99.75	9.89	0.812

Table 3 | Thermodynamic results of phosphate adsorbed by CCMA-0.83-600

Temperature (K)	$\triangle G$ (kJ/mol)	$\triangle H$ (kJ/mol)	$\triangle S$ (J/mol/K)
288.15	−1.067	81.77	286.78
298.15	−3.631		
308.15	−6.816		

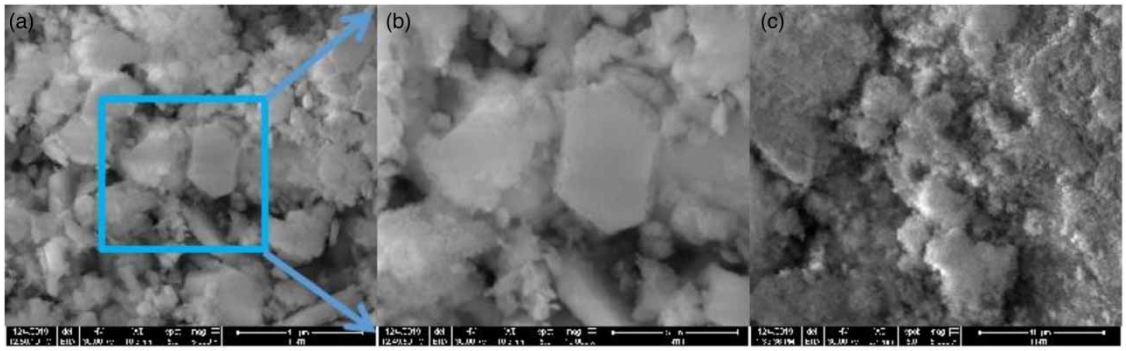

Figure 7 | SEM of CCMA-0.83-600 before (a,b) and after (c) the adsorption of phosphate.

after phosphorus adsorption, CCMA-0.83-600 reverted to the original layered structure. Some phosphate would be adsorbed on the surface of CCMA-0.83-600 by the van der Waals force which belonged to physical adsorption. (2) Anion intercalation plays an important role in the process of phosphate adsorbed by CCMA-0.83-600. The characteristic diffraction peak of boehmite appeared on the XDR spectrum of CCMA-0.83-600 after the adsorption of phosphate. The corresponding d value of the (002) crystal plane exhibited 7.7939 Å, which was higher than that before adsorption ($d = 7.7801$ Å), indicating that CCMA-0.83-600 recovered the original layered structure in the phosphate solution. The phosphate radical entered the interlayer through intercalation and increased the interlayer spacing. (3) Ion exchange: As for CCMA-0.83-600, ion exchange refers to that after the calcined LDHs are restored to layered structure in solution, and the interlayer anions are replaced by anions with stronger exchange performance. To explore whether ion exchange was involved in the phosphate adsorption process, the changes of phosphate and Cl^- as well as pH changes were determined in distilled water and the phosphate solution. The release rate of Cl^- ranging CCMA-0.83-600 in distilled water was much lower than that in the phosphate solution, indicating that phosphate ions entered the interlayer to replace Cl^- in the phosphate solution, resulting in an accelerated release rate of Cl^- (Table 4). That is, ion exchange was involved in the process of phosphate adsorbed by CCMA-0.83-600, which was also further confirmed by the FT-IR result (Figure 8(b)). The FT-IR spectrum of CCMA-0.83-600 after adsorbing phosphate gives the stretching vibration peak and bending vibration peak of phosphate at around 3,499 and 3,493 cm^{-1}. The band at 876 cm^{-1} is associated with the vibration of P–O of HPO_4^{2-}, demonstrating that phosphate has been successfully adsorbed

Table 4 | The concentration of phosphate, Cl− and pH changes in the process of phosphate adsorbed by CCMA-0.83-600

	Distilled water		Phosphate-containing solution			
Reaction time (min)	The concentration of Cl^- (mg/L)	pH	The concentration of phosphate (mg/L)	The concentration of Cl^- (mg/L)	pH	$P_{in}/(Cl^-_{phosphate\ out}$-$Cl^-_{balnk\ out})$ molar ratio
0	0	7	100	0	4	0
5	0	9.12	71.86	0	7.10	5.70
10	2.22	10.15	56.71	7.16	7.95	4.28
30	3.63	10.37	31.95	12.11	8.87	3.43
60	4.24	10.33	21.62	19.93	9.25	2.78
120	4.68	10.17	13.42	24.08	9.27	2.32
180	4.72	9.82	8.92	27.65	9.26	1.93
240	4.91	9.68	5.13	30.17	9.22	1.94
300	5.02	9.56	2.59	32.23	9.09	1.22
360	5.13	9.32	1.13	34.42	9.01	1.26
420	5.21	9.21	0.46	35.66	8.96	0.92
480	5.31	8.97	0.42	36.49	8.89	0.40
540	5.51	8.82	0.42	36.79	8.85	0

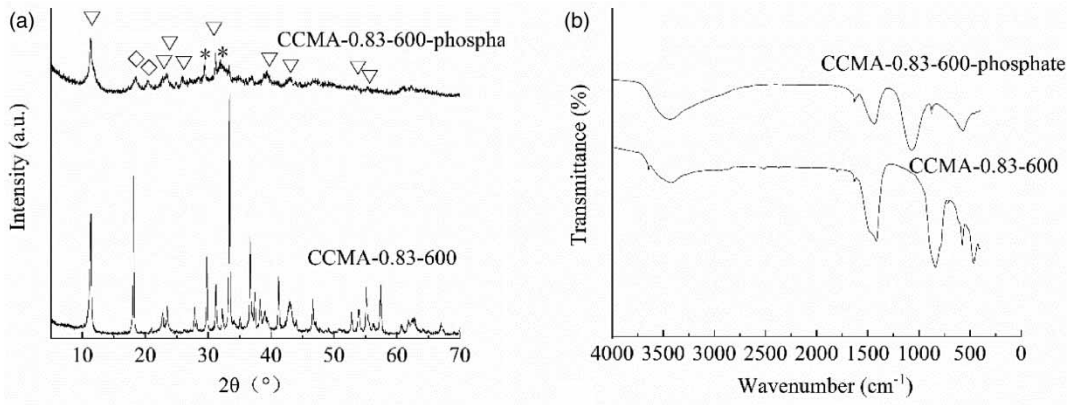

Figure 8 | XRD (a) and FT-IR (b) patterns of CCMA-0.83-600 before and the after adsorption of phosphate.

by CCMA-0.83-600 and ion exchange participated in this process. (4) Surface coordination: LDHs have metal hydroxide laminates, and the calcined products are metal oxides. The surfaces of metal oxides and metal hydroxides both have the ≡MOH group which can coordinate with phosphate to generate various coordination complexes as Equations (5)–(9). (5) Chemical precipitation: The calcined LDHs will recover their original layered structure through rehydration in an acidic solution. In this process, some free metal cations will be generated, and these free metal cations will combine with phosphate adsorbed on the adsorbent surface to form various phosphate precipitates. Compared to CCMA-0.83-600 (Figures 7(a) and 7(b)), the surface of CCMA-0.83-600 was relatively flat after adsorbing phosphate (Figure 7(c)), which might be due to the deposition of phosphate and metal hydroxides formed by the combination of free metal cations with phosphate and hydroxyl groups. Besides, the characteristic peak of $Ca_2P_2O_7$ was detected on the XRD spectrum of CCMA-0.83-600 after the phosphate adsorption through the precipitation between Ca^{2+} and $P_2O_7^{2-}$ (Figure 8(a)). Based on the above discussion, the adsorption mechanism could be described in Figure 9.

$$\equiv MeOH + PO_4^{3-} = \equiv MePO_4^{2-} + OH^- \tag{12}$$

$$2 \equiv MeOH + PO_4^{3-} = (\equiv Me)_2PO_4^- + 2OH^- \tag{13}$$

$$\equiv MeOH + HPO_4^{2-} = \equiv MeHPO_4^- + OH^- = \equiv MePO_4^{2-} + H_2O \tag{14}$$

$$\equiv MeOH + H_2PO_4^- = \equiv MeH_2PO_4 + OH^- = \equiv MeHPO_4^- + H_2O \tag{15}$$

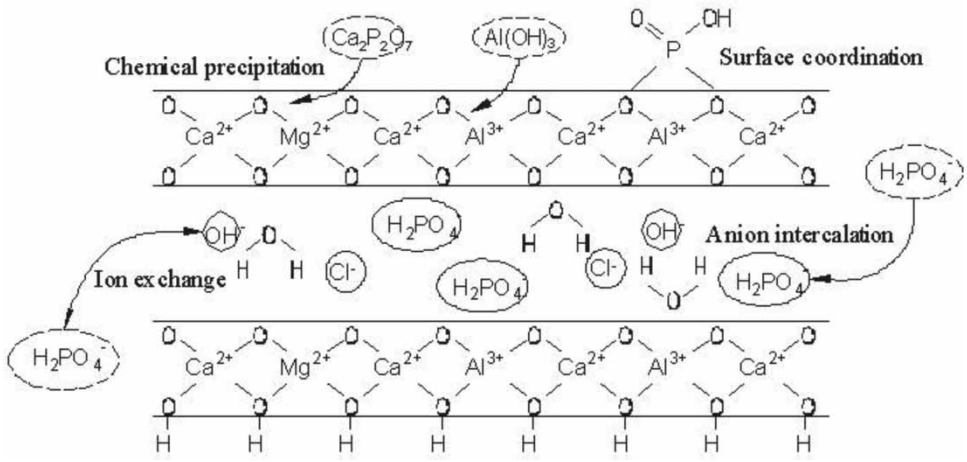

Figure 9 | Mechanism of adsorption of phosphate by CCMA-0.83-600.

4. CONCLUSION

In this study, a nanocomposite CCMA-0.83-600 was designed via a constant pH double titration coprecipitation to prepare a new type of hydrocalumite structure of CaMgAl-LDHs phosphate adsorption materials. The obtained CaMgAl-LDHs were further calcined at 600 °C to prepare CCMA-0.83-600. The XRD and SEM analysis indicated that the prepared CCMA-0.83-600 had typical characteristics of LDHs. The adsorption process of phosphate by CCMA-0.83-600 follows the pseudo-second-order kinetic model, and the adsorption rate was controlled by both the liquid film diffusion and intra-particle diffusion. The adsorption accords with the Langmuir model, adsorption $R^2 > 0.99$, and the n value of the Freundlich model was greater than 2, indicating that phosphate was easily adsorbed by CCMA-0.83-600. The saturated adsorption capacity at 15, 25 and 35 °C was 130.79, 149.91 and 161.66 mg/g, respectively. Thermodynamic calculation results showed that $\triangle G < 0$, $\triangle H > 0$, $\triangle S > 0$ indicating the adsorption was a spontaneous endothermic reaction, increasing the temperature was beneficial for the positive direction of adsorption, and that the confusion degree of the system increased and the orderliness decreased during the adsorption process. The static adsorption experiment and microscopic analysis showed that the adsorption of phosphate by CCMA-0.83-600 was the result of physical adsorption, anion intercalation, ion exchange, surface coordination and chemical precipitation. CCMA-0.83-600 is an excellent adsorbent material for the treatment of phosphorus wastewater and is worthy of widespread popularization and application.

ACKNOWLEDGEMENTS

This work was supported by the Shandong Provincial Natural Science Foundation (NO. ZR2021ME038, ZR2021QE272 and ZR2021QE087) and the National Natural Science Foundation of China (NO. 51474122).

DATA AVAILABILITY STATEMENT

All relevant data are included in the paper or its Supplementary Information.

CONFLICT OF INTEREST

The authors declare there is no conflict.

REFERENCES

Cao, H., Wu, X., Syed-Hassan, S. S. A., Zhang, S., Mood, S. H., Milan, Y. J. & Garcia-Perez, M. 2020 Characteristics and mechanisms of phosphorous adsorption by rape straw-derived biochar functionalized with calcium from eggshell. *Bioresource Technology* **318**, 124063.

Cheng, X., Huang, X., Wang, X., Zhao, B., Chen, A. & Sun, D. 2009 Phosphate adsorption from sewage sludge filtrate using zinc–aluminum layered double hydroxides. *Journal of Hazardous Materials* **169**, 958–964.

Guo, Y., Chen, W., Cao, Y. & Li, G. 2021 Enhanced adsorptive removal of phosphate on calcined Zr-modified layered double oxide. *Desalination and Water Treatment* **238**, 251–259.

Khajeh, M., Oveisi, A. R., Barkhordar, A., Rakhshanipour, M. & Sargazi-Avval, H. 2022 Ternary NiCuZr layered double hydroxide@MIL-101 (Fe)-NH_2 metal-organic framework for photocatalytic degradation of methylene blue. *Journal of Nanostructure in Chemistry* **12**, 105–115.

Kong, Q., Shi, X., Ma, W., Zhang, F., Yu, T., Zhao, F., Zhao, D. & Wei, C. 2021 Strategies to improve the adsorption properties of graphene-based adsorbent towards heavy metal ions and their compound pollutants: a review. *Journal of Hazardous Materials* **415**, 125690.

Kong, Q., Zhang, H., Lan, Y., Shi, X., Fang, Z., Chang, Q., Liu, J. & Wei, C. 2022 Functional graphene oxide for organic pollutants removal from wastewater: a mini review. *Environmental Technology*, 1–13, ahead-of-print. 10.1080/09593330.2022.2053754

Li, R., Wang, J. J., Zhou, B., Awasthi, M. K., Ali, A., Zhang, Z., Gaston, L. A., Lahori, A. H. & Mahar, A. 2016 Enhancing phosphate adsorption by Mg/Al layered double hydroxide functionalized biochar with different Mg/Al ratios. *Science of the Total Environment* **559**, 121–129.

Lyu, P., Li, L., Huang, X., Wang, G. & Zhu, C. 2022 Pre-magnetic bamboo biochar cross-linked Ca Mg Al layered double-hydroxide composite: high-efficiency removal of As(III) and Cd(II) from aqueous solutions and insight into the mechanism of simultaneous purification. *Science of the Total Environment* **823**, 153743.

Manobala, T., Shukla, S. K., Rao, T. S. & Kumar, M. D. 2021 Kinetic modelling of the uranium biosorption by *Deinococcus radiodurans* biofilm. *Chemosphere* **269**, 128722.

Seftel, E. M., Ciocarlan, R. G., Michielsen, B., Meynen, V., Mullens, S. & Cool, P. 2018 Insights into phosphate adsorption behavior on structurally modified ZnAl layered double hydroxides. *Applied Clay Science* **165**, 234–246.

Wang, Y., Xie, X., Chen, X., Huang, C. & Yang, S. 2020 Biochar-loaded Ce^{3+}-enriched ultra-fine ceria nanoparticles for phosphate adsorption. *Journal of Hazardous Materials* **396**, 122626.

Wu, W., Wu, Y., Jin, B. & Gu, Q. 2019 Synthesis, characterization, and high-temperature HCl capture capacity of different proportions of potassium fluoride-doped CaMgAl layered double hydroxides. *ACS Omega* **4**, 18159–18166.

Xiao, L., Li, P., Kong, Q. & Lan, Y. 2021 From wastes to functions: preparation of layered double hydroxides from industrial waste and its removal performance towards phosphates. *Environmental Science and Pollution Research* **29**, 11893–11906.

Zhang, Z., Yan, L., Yu, H., Yan, T. & Li, X. 2019 Adsorption of phosphate from aqueous solution by vegetable biochar/layered double oxides: fast removal and mechanistic studies. *Bioresource Technology* **284**, 65–71.

Zhang, J., Xia, Q., Hong, X., Chen, J. & Liu, D. 2021 Synthesis of layered double hydroxides with nitrate and its adsorption properties of phosphate. *Water Science and Technology* **83**, 100–110.

Zhou, J. Z., Xu, Z. P., Qiao, S., Liu, J., Liu, Q., Xu, Y., Zhang, J. & Qian, G. 2011 Triphosphate removal processes over ternary CaMgAl-layered double hydroxides. *Applied Clay Science* **54**, 196–201.

First received 21 November 2022; accepted in revised form 23 December 2022. Available online 13 January 2023